

Strain- and electric field-induced band gap modulation in nitride nanomembranes

This article has been downloaded from IOPscience. Please scroll down to see the full text article.

2013 J. Phys.: Condens. Matter 25 195801

(<http://iopscience.iop.org/0953-8984/25/19/195801>)

View [the table of contents for this issue](#), or go to the [journal homepage](#) for more

Download details:

IP Address: 141.219.155.120

The article was downloaded on 20/04/2013 at 19:57

Please note that [terms and conditions apply](#).

Strain- and electric field-induced band gap modulation in nitride nanomembranes

Rodrigo G Amorim¹, Xiaoliang Zhong¹, Saikat Mukhopadhyay¹, Ravindra Pandey¹, Alexandre R Rocha^{2,3} and Shashi P Karna⁴

¹ Department of Physics, Michigan Technological University, Houghton, MI 49931, USA

² Centro de Ciências Naturais e Humanas, Universidade Federal do ABC, Santo André, SP, Brazil

³ Instituto de Física Teórica, Universidade Estadual Paulista (UNESP), São Paulo, SP, Brazil

⁴ US Army Research Laboratory, Weapons and Materials Research Directorate, ATTN: RDL-WM, Aberdeen Proving Ground, MD 21005-5069, USA

E-mail: pandey@mtu.edu


Received 30 October 2012, in final form 7 March 2013

Published 19 April 2013

Online at stacks.iop.org/JPhysCM/25/195801

Abstract

The hexagonal nanomembranes of the group III-nitrides are a subject of interest due to their novel technological applications. In this paper, we investigate the strain- and electric field-induced modulation of their band gaps in the framework of density functional theory. For AlN, the field-dependent modulation of the bandgap is found to be significant whereas the strain-induced semiconductor-metal transition is predicted for GaN. A relatively flat conduction band in AlN and GaN nanomembranes leads to an enhancement of their electronic mobility compared to that of their bulk counterparts.

 Online supplementary data available from stacks.iop.org/JPhysCM/25/195801/mmedia

(Some figures may appear in colour only in the online journal)

1. Introduction

Monolayer materials such as graphene have opened up the possibility of novel and cost-effective applications in the areas of electronic and photonics [1–4]. In order to envision an even larger spectrum of applications of monolayers, one generally requires the monolayer to have a finite bandgap. For graphene, the bandgap opens up under the application of an external field [5, 6], though the magnitude of the gap is about a few-hundred meV [7]. Alternatively, it has been suggested that the hexagonal monolayer structure with the broken sublattice symmetry can be considered for device applications, e.g. a monolayer with two different types of atoms such as boron and nitrogen [8–11].

Advances in experimental techniques such as exfoliation and epitaxial lift-off have, in fact, allowed fabrication of novel planar structures, which, in principle, do not occur naturally, albeit based on conventional materials [12, 13]. Such new planar structures of semiconducting materials—referred to

as nanomembranes—have been fabricated in the isolated or free-standing form with the mono-crystalline 2D-layer structures with thickness of 5–500 nm, and large lateral dimensions which are generally two orders of magnitude greater than the thickness for the particular case of oxides and nitrides [8–19, 9, 20–22]. It is to be noted that the ultimate one-atom-thick limit has been reached for the cases of BN [8–11], ZnO [13] and Si [21], all in a hexagonal honeycomb arrangement similar to that of graphene.

In the particular case of h-BN, experimental [20] and theoretical [9, 23] investigations have been performed either in the isolated form for electronic and optoelectronic applications or as a scaffold for altering the properties of graphene [24, 25]. In the nitride family, the other members including AlN and GaN are the well-known semiconductors. Nanomembranes of both AlN and GaN have already been fabricated [26], albeit not in the one-atom-thick limit. At the same time, the bulk nitrides prefer the wurtzite structure in their ground state configurations, as also the case with

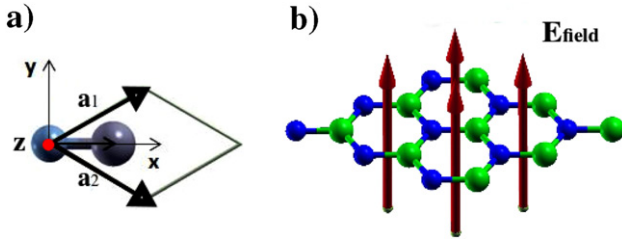


Figure 1. A schematic diagram of the (a) unit cell, and (b) super cell of the hexagonal nitride nanomembranes (N-Green, cation (B/Al/Ga)-Blue). The vertical arrows in (b) show the direction of the applied electric field.

ZnO which has been synthesized in a hexagonal monolayer arrangement [27]. Consequently, a systematic and detailed study of the nitride nanomembranes is essential considering that realization of the nanomembrane-based devices requires a comprehensive knowledge of their structural, mechanical and electronic properties.

In this paper, we report the results of a theoretical study based on density functional theory (DFT) on the graphene-like configurations of AlN and GaN. The calculated results on the BN monolayer will be used to benchmark our modeling elements. Our aim will be to quantify the differences between the 2D-planar structures and their bulk counterparts in terms of structural, mechanical and electronic properties. Most importantly, we will investigate tuning of the bandgaps of the nanomembranes with two distinct approaches, namely mechanical strain and electric field. We will show that, while BN has been widely considered as a potential candidate for applications [10, 18, 19, 9, 20, 23, 28–30], pristine AlN and GaN monolayer configurations present a more pronounced dependence on strain and transverse electric field, thus emerging as promising candidates for novel technological applications.

2. Methodology

Nanomembranes considered in this study are derived from the group III–V nitrides and have the graphene-like hexagonal 2D lattice consisting of two sublattices namely N and X (X being B, Al, or Ga). A schematic representation of the unit cell and the corresponding super cell is shown in figure 1.

Electronic structure calculations were performed using density functional theory (DFT) [31] as implemented in the SIESTA program package [32]. The Kohn–Sham equations were solved in the full self-consistent manner with double-zeta polarized numerical basis set and norm-conserving pseudo-potentials. The generalized gradient approximation for the exchange and correlation potential using the Perdew–Burke–Ernzerhof (PBE) functional form [33] was employed. A vacuum distance of 12 Å, between neighboring systems images in the perpendicular direction to nanomembrane sheet, was used to avoid image interactions. The k -space integration was done with a grid of $9 \times 9 \times 1$ k -points and all structures were fully relaxed until the residual forces were smaller than $0.01 \text{ eV } \text{Å}^{-1}$.

Table 1. Intraplanar bond length, lattice constant and cohesive energy of BN, AlN and GaN nanomembranes.

Nanomembrane	(Intraplanar) bond length R (Å)	(Intraplanar) lattice constant a (Å)	Cohesive energy E_{coh} (eV/atom)
BN	1.45	2.509	7.81
AlN	1.82	3.159	4.94
GaN	1.91	3.301	3.62

Our aim is to investigate how one can tune the bandgaps of nanomembranes in two aspects: homogeneous strain and perpendicular electric field. Firstly, we considered isotropic changes in each lattice vector (a_1 and a_2) for strain calculations as can be seen in figure 1. Considering these homogeneous changes of the system, one can describe both the compression and expansion effects. Secondly, an additional term in the Hamiltonian that describes a constant external field is used for the case of the applied electric field. Due to the use of periodic boundary conditions even in the perpendicular direction, a saw-tooth potential profile perpendicular to the membrane is included to take into account the effect of the homogeneous electric field. The whole system was placed in the middle of the simulated box. A full geometrical optimization of the simulation box under the effect of the electric field yielded negligible changes to the atomic arrangements. For example, a very small buckling ($\approx 0.14 \text{ Å}$) accompanied by a change in the bond length of about $+0.27\%$ was induced by the electric field of $2 \text{ V } \text{Å}^{-1}$ in the AlN nanomembrane.

3. Results and discussion

3.1. Structural properties

The equilibrium structural parameters of the nitride nanomembranes are collected in table 1. Note that the fully optimized hexagonal configurations retain the symmetry of the graphene-like structure.

The calculated intraplanar bond length (i.e. nearest-neighbor distance, R) increases in going from BN to AlN to GaN. $R_{\text{B–N}}$ of 1.45 Å is slightly larger than the typical value of 1.42 Å of the sp^2 hybridized carbon configuration, and is in agreement with the results of previous theoretical DFT studies [23]. The calculated lattice constants are 2.509, 3.159 and 3.301 Å for the BN, AlN and GaN nanomembranes, respectively. Interestingly, these 2D materials have similar lattice constants compared with their 3D counterparts, in spite of a different atomic coordination number. The lattice constants of the wurtzite BN, AlN and GaN were reported to be 2.54, 3.06 and 3.17 Å , respectively [34].

The cohesive energies per atom for BN, AlN, and GaN nanomembranes are found to be 7.81, 4.94, and 3.65 eV, respectively suggesting the B–N bond to be the strongest followed by the Al–N and Ga–N bonds. We define the cohesive energy as the difference between total energy of a

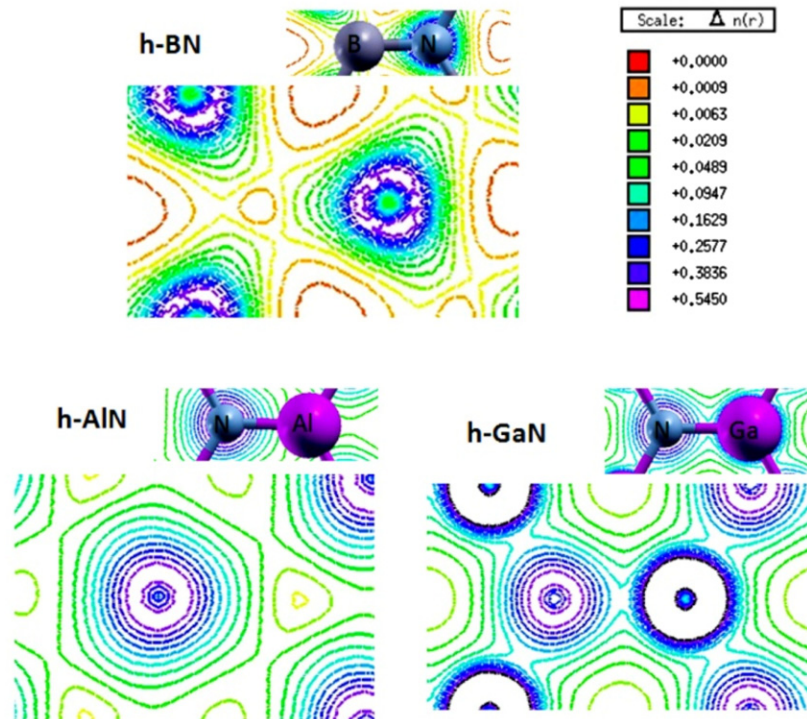


Figure 2. The valence charge density plots (in electrons/bohr³) of BN, AlN and GaN nanomembranes.

nanomembrane and the sum of total energies of corresponding constituent atoms⁵.

The trend in the cohesive energy can be correlated with the nature of chemical bonds as demonstrated by the contour plots of the charge density (figure 2). For BN, the presence of directional bonds indicates their nature to be covalent with sharing of electrons among B and N-atoms with a considerable overlap of their electronic wavefunctions. Conversely, the bonds have more ionic character in AlN due to a charge transfer from Al to N, which leads to localized wavefunctions (shown as concentric spheres in figure 2) centered at the N-atoms with no significant overlap of the two neighboring spherical islands. For the GaN nanomembrane, we found localization of the electronic wavefunction, similar to the case of AlN, but with a smaller degree of distortion together with a smaller overlap in the wavefunction centered at Ga and N (figure 2). Consequently the bonding in GaN could be considered to be partly ionic and partly covalent.

3.2. Electronic properties

The electronic band structures of the nitride nanomembranes are presented in figure 3. The minimum energy gaps for BN, AlN and GaN are calculated to be 4.60, 3.06 and 1.70 eV, respectively. The valence band maximum (VBM) is located at the high-symmetry K point for all configurations whereas the conduction band minimum (CBM) is at K for BN, and Γ for AlN and GaN. Therefore, a direct bandgap is predicted for BN whereas indirect band gaps are predicted

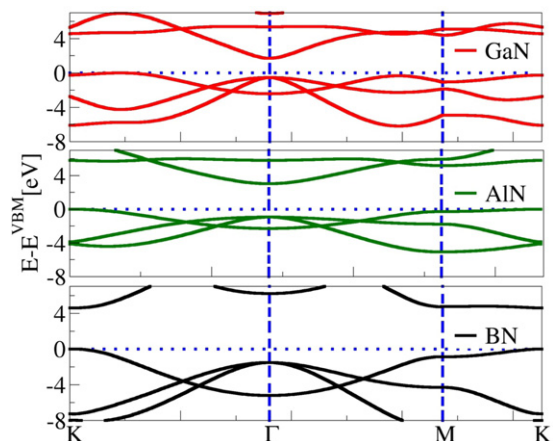


Figure 3. The calculated band structures of the BN, AlN and GaN nanomembranes.

for AlN and GaN. This is in contrast to what has been reported for the bulk wurtzite nitrides with the gap being indirect for BN and direct for AlN and GaN [35]. The difference in the nature of the bandgap can be attributed to a shift in the position of the VBM—from Γ to K—when the dimensionality is reduced, whereas the character of the CBM remains unchanged. Nevertheless, the calculated magnitude of the minimum bandgap of the nanomembranes follows the same order as predicted for their bulk counterparts [35].

The calculated density of states (DOS) and partial DOS are shown in figure 4. VBM is mainly composed of N-p orbitals, with a small contribution from the cation-p orbitals. The conduction band minimum of BN is composed of the B-p

⁵ Note that spin-polarized electronic structure calculations were performed to obtain atomic energies for B, Al, Ga and N, (n.d.).

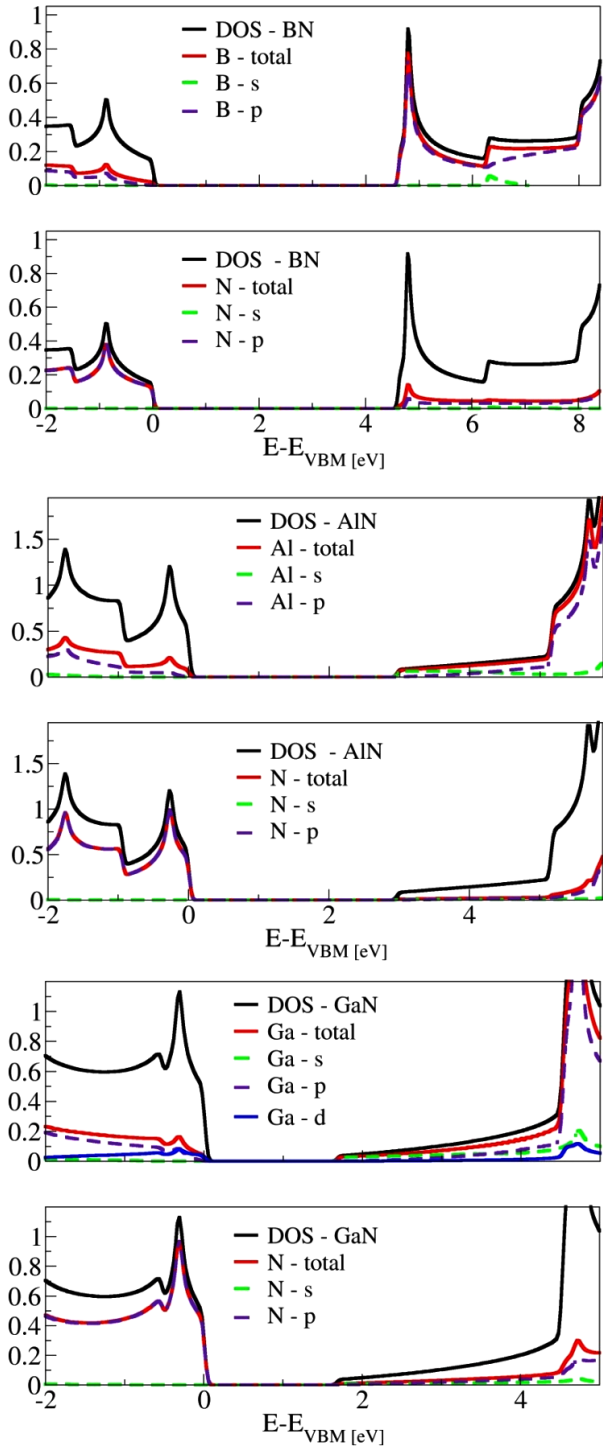


Figure 4. Total and projected density of states of the BN, AlN and GaN nanomembranes.

orbitals whereas that of AlN (GaN) is mainly composed of Al-s (Ga-s) orbitals.

The most significant and advantageous change, which the nitride nanomembranes undergo due to the reduced dimensionality, is the enhancement of their electronic mobility. The electron effective mass is calculated to be 0.14 and 0.06 m_0 for AlN and GaN, respectively, where m_0 is the free electron mass. Note that the electron effective

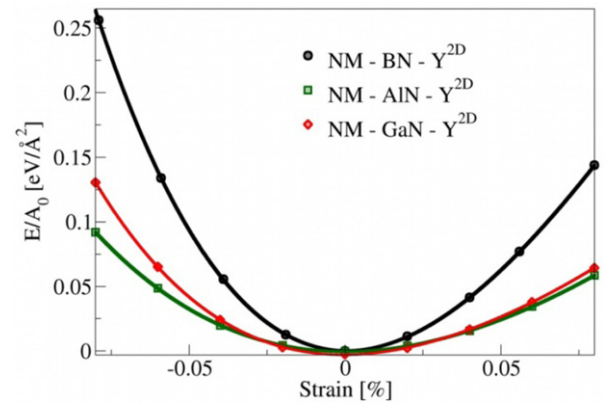


Figure 5. Energy versus the applied strain for the BN, AlN and GaN nanomembranes.

mass is formally the reciprocal of the second derivative of the energy–momentum relation. Compared with GaN, the relatively larger electron effective mass of AlN is directly related to the flatness of the energy curve around CBM (figure 3). On the other hand, the hole effective mass is calculated to be 0.43 and 0.36 m_0 for AlN and GaN, respectively. For comparison, the theoretical (experimental) values of the electron effective mass are reported to be 0.23 m_0 [37] (0.29–0.4 m_0 [37, 38]) and 0.14 m_0 [36] (0.22 m_0 [37]) for the wurtzite AlN and GaN, respectively.

3.3. In-plane stiffness

We define a ‘biaxial modulus’ to characterize the in-plane isotropic stiffness of the considered nanomembranes. The so-called biaxial modulus is defined as, $Y_{2D} = \frac{1}{A} \left(\frac{\partial^2 E}{\partial \epsilon^2} \right) \Big|_{\epsilon=0}$, where E is the total energy, ϵ is the biaxial strain and A_0 the equilibrium area of the unit cell. The ‘biaxial modulus’ is analogous to the two-dimensional Young’s modulus, which is related to the uniaxial strain [39].

In our case, the in-plane strain (ϵ) is simulated by varying the lattice constant from -8% to $+8\%$ away from its equilibrium value while all bond angles are kept fixed. Thus, a biaxial strain is considered whereby the entire lattice is uniformly stretched. This uniform strain could be obtained, for instance, by synthesizing the nanomembrane on top of a material that has a lattice mismatch. From our definition, ‘negative’ strain is considered as the strain by compression and ‘positive’ strain is considered as the tensile strain for the nanomembrane.

The corresponding total energy curves as a function of strain are shown in figure 5. The calculated values of the biaxial modulus are 384, 142 and 178 N m^{-1} for BN, AlN and GaN nanomembranes, respectively. These results follow the same hierarchy as the strength of their interatomic bonds (table 1). For comparison, the bulk moduli follow a similar order with the values of 400, 207, and 245 GPa for BN [40], AlN [41], and GaN [42], respectively. Consequently, one can conclude that the nitride nanomembranes, specifically AlN and GaN are significantly more malleable than their bulk counterparts. We believe that the malleability of AlN and

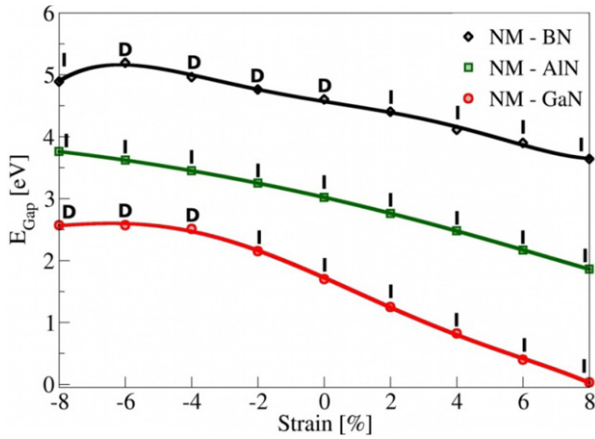


Figure 6. The calculated bandgap versus the applied strain for the BN, AlN and GaN nanomembranes.

GaN together with the enhanced electron mobility make these systems attractive for flexible electronics [12].

3.4. Strain-modulated bandgap

Considering that the application of strain can affect the electronic properties of a given system, we now investigate the effect of strain applied to the nanomembranes on their energy gaps. For the case of in-plane tensile strain (i.e. $\varepsilon > 0$), a consistent reduction in bandgap with increasing strain is predicted (figure 6).

Elongation of the bond length under tensile strain modifies the orbital hybridization of neighboring atoms, thereby facilitating tunability of their band gaps. Both BN and AlN show a smaller degree of tunability with tensile strain. However, a direct–indirect band transition (from K–K to K–M) is noted for BN, which is related to the variation of orbital composition of the VBM states with the applied tensile strain. This is not the case with AlN where no such transition in the bandgap with the applied tensile strain is noted.

A significant tunability with the strain is predicted for GaN, which also goes through a semiconductor–semimetal transition at the value of +8%. This transition can be attributed to reduction of the overlap of the orbitals due to an increase in the Ga–N bond length in the strained lattice. In particular, the Ga-s-like conduction band around Γ shifts downwards until it eventually closes the gap (see supplementary figure S1 available at stacks.iop.org/JPhysCM/25/195801/mmedia). Our results are consistent with the previous results on graphitic GaN multi-layer films where the bandgap was reported to decrease linearly with the tensile strain [33].

Application of an in-plane compressive strain (i.e. $\varepsilon < 0$) to the nanomembranes increases their band gaps. A shortening of the bond length increases the repulsion between orbitals associated with the neighboring atoms resulting in the reorganization of the bands away from the Fermi level. For GaN, it leads to an indirect–direct gap transition at about –4% as VBM moves from K to Γ . The valence wavefunctions at Γ are initially doubly degenerate; one level is due to N- p_z

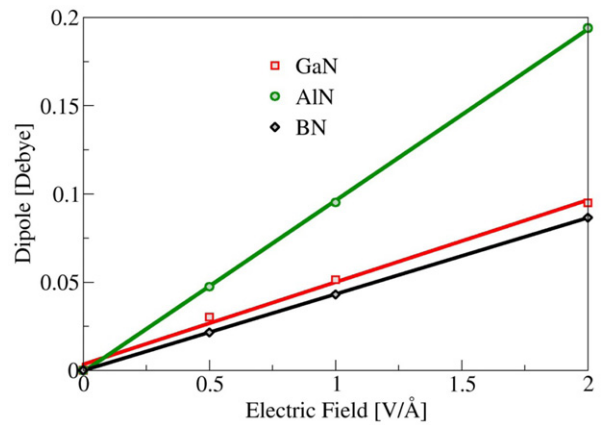
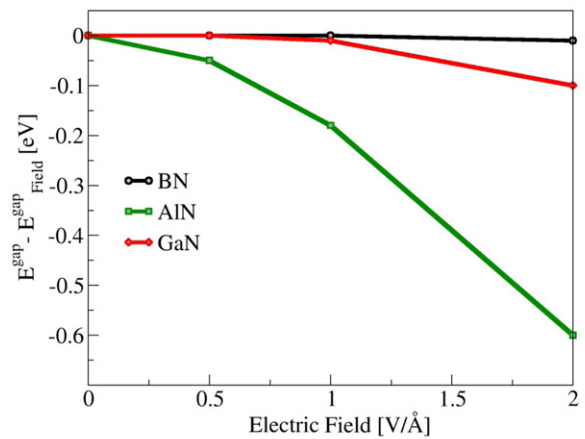


Figure 7. The variation of bandgap (top) and dipole field (bottom) with the applied electric field for the BN, AlN and GaN nanomembranes.

whereas the other has an in-plane nitrogen p_x – p_y character. After the application of the compressive strain, p_z -orbitals shift down and the p_x – p_y orbitals move upward to become the CBM, consequently leading to the direct–indirect bandgap transition. The direct–indirect transition (from K–K to Γ –K) predicted for BN at higher compressive strains has a similar origin, i.e., from the splitting and subsequent upward shift of the levels at Γ . No change in the nature of the gap in AlN is predicted for either compressive or tensile strain applied to the system.

3.5. Field-modulated band gap

The effects of an electric field applied perpendicular to the nanomembranes on the electronic properties are shown in figure 7(a). A prominent variation of the bandgap is predicted for AlN as compared to that for BN or GaN. This is accompanied by a noticeable change in the dipole moment of AlN (figure 7(b)), and may be attributed to the nature of its chemical bond. A higher degree of electronic polarization in the electric field is facilitated by the ionic bond, which in turn, leads to a significant variation of the bandgap of AlN under the application of the external electric field.

It is to be noted that the maximum value of $2 \text{ V } \text{\AA}^{-1}$ considered for the perpendicular electric field appears to be

high. However, a nanomembrane should be able to sustain such a high field since the electrical field is likely to induce changes in the charge density within a 2–3 Å around the nanomembrane. Furthermore, Britnell *et al* [43], found the breakdown voltage of $\sim 1 \text{ V nm}^{-1}$ (1 GV m^{-1}) for the system consisting of a few layers of h-BN sheet sandwiched between two gold electrodes. In experiments h-BN was used as a dielectric sandwiched between the metallic electrodes. The simulation model, on the other hand, employs a free-standing nanomembrane in vacuum which works as the dielectric. Thus, given the differences in configurations considered for experiment and simulation, the applied field of 2 V Å^{-1} can be taken as the maximum value of the breakdown voltage for the ‘isolated’ nanomembrane.

A comparison of the effects of induced strain and applied electric field suggests that the strain-engineered tailoring of the bandgap is a more effective approach for the nitride nanomembranes. Application of the perpendicular electric field only shifts the states relative to the Fermi energy without changing the nature of the bands (i.e. the Stark effect). A tunability of the bandgap therefore depends upon the magnitude of dipole moments along the direction of the field. Introduction of the in-plane strain, however, changes the nature of the bands in addition to shifting them near the Fermi energy.

4. Summary

In summary, we have performed density functional theory calculations of one-atom-thick nitride nanomembranes, BN, AlN and GaN. We predict that the bandgap of these ultra-thin hexagonal structures can be modulated by either in-plane strain or a transverse electric field. For BN and GaN, the variation of the gap is non-monotonic with respect to the compressive strain, though the nature of the gap changes from direct to indirect or *vice versa*. This effect is attributed to shifts in either the conduction or the valence band and to subsequent changes in the character of the CBM and VBM depending on the magnitude of the strain applied. In the case of a transverse electric field, AlN, which has a more ionic character, shows a higher dependence on the electric field associated with significant changes to its out-of-plane dipole moment. The predicted tunability of the bandgap by using either strain or a transverse electric field is therefore likely to lead to a wide range of possible applications of the nitride nanomembranes in electronic devices.

Acknowledgments

We acknowledge support from Brazilian Agencies CNPQ and FAPESP and computational resources CENAPAD/SP and NACAD/UFRJ. The work at Michigan Technological University was performed under support by the Army Research Office through Contract Number W911NF-09-1-0221.

References

- [1] Geim A K and Novoselov K S 2007 The rise of graphene *Nature Mater.* **6** 183–91
- [2] Schedin F *et al* 2007 Detection of individual gas molecules adsorbed on graphene *Nature Mater.* **6** 652–5
- [3] Schwierz F 2010 Graphene transistors *Nature Nanotechnol.* **5** 487–96
- [4] Kim K, Choi J Y, Kim T, Cho S H and Chung H J 2011 A role for graphene in silicon-based semiconductor devices *Nature* **479** 338–44
- [5] Cocco G and Cadelano E 2010 Gap opening in graphene by shear strain *Phys. Rev. B* **81** 241412
- [6] Wong J, Wu B and Lin M F 2012 Strain effect on the electronic properties of single layer and bilayer graphene *J. Phys. Chem. C* **116** 8271–7
- [7] Bourzac K 2012 Back to analogue *Nature* **483** 534
- [8] Novoselov K S *et al* 2005 Two-dimensional atomic crystals *Proc. Natl Acad. Sci. USA* **102** 10451–3
- [9] Zhi C, Bando Y, Tang C, Kuwahara H and Golberg D 2009 Large-scale fabrication of boron nitride nanosheets and their utilization in polymeric composites with improved thermal and mechanical properties *Adv. Mater.* **21** 2889–93
- [10] Qin L, Yu J, Li M, Liu F and Bai X 2011 Catalyst-free growth of mono- and few-atomic-layer boron nitride sheets by chemical vapor deposition *Nanotechnology* **22** 215602
- [11] Kim K K *et al* 2012 Synthesis of monolayer hexagonal boron nitride on Cu foil using chemical vapor deposition *Nano Lett.* **12** 161–6
- [12] Rogers J A, Lagally M G and Nuzzo R G 2011 Synthesis, assembly and applications of semiconductor nanomembranes *Nature* **477** 45–53
- [13] Tusche C and Meyerheim H 2007 Observation of depolarized ZnO(0001) monolayers: formation of unreconstructed planar sheets *Phys. Rev. Lett.* **99** 026102
- [14] Paskiewicz D M, Scott S A, Savage D E, Celler G K and Lagally M G 2011 Symmetry in strain engineering of nanomembranes: making new strained materials *ACS Nano* **5** 5532–42
- [15] Zhang P *et al* 2006 Electrical conductivity in silicon nanomembranes *New J. Phys.* **8** 200
- [16] Lee K J *et al* 2006 Bendable GaN high electron mobility transistors on plastic substrates *J. Appl. Phys.* **100** 124507
- [17] Chung K, Lee C H and Yi G C 2010 Transferable GaN layers grown on ZnO-coated graphene layers for optoelectronic devices *Science* **330** 655–7
- [18] Pacilé D, Meyer J C, Girit C O and Zettl A 2008 The two-dimensional phase of boron nitride: few-atomic-layer sheets and suspended membranes *Appl. Phys. Lett.* **92** 133107
- [19] Han W Q, Wu L, Zhu Y, Watanabe K and Taniguchi T 2008 Structure of chemically derived mono- and few-atomic-layer boron nitride sheets *Appl. Phys. Lett.* **93** 223103
- [20] Alem N, Erni R, Kisielowski C and Rossell M 2009 Atomically thin hexagonal boron nitride probed by ultrahigh-resolution transmission electron microscopy *Phys. Rev. B* **80** 155425
- [21] Vogt P, Padova P D, Quaresima C, Avila J and Frantzeskakis E 2012 Silicene: compelling experimental evidence for graphene-like two-dimensional silicon *Phys. Rev. Lett.* **108** 155501
- [22] Zhou H, Seo J H, Paskiewicz D M, Zhu Y, Celler G K, Voyles P M, Zhou W, Lagally M G and Ma Z 2013 Fast flexible electronics with strained silicon nanomembranes *Sci. Rep.* **3** 1291
- [23] Azevedo S, Kaschny J R, de Castilho C M C and de Brito Mota F 2009 Electronic structure of defects in a boron nitride monolayer *Eur. Phys. J. B* **67** 507–12

- [24] Liu Z, Song L, Zhao S, Huang J and Ma L 2011 Direct growth of graphene/hexagonal boron nitride stacked layers *Nano Lett.* **11** 2032–7
- [25] Kan E *et al* 2012 Why the band gap of graphene is tunable on hexagonal boron nitride *J. Phys. Chem. C* **116** 3142
- [26] Mei Y *et al* 2009 Fabrication, self-assembly, and properties of ultrathin AlN/GaN porous crystalline nanomembranes: tubes, spirals, and curved sheets *ACS Nano* **3** 1663–8
- [27] Tusche C, Meyerheim H L and Kirschner J 2007 Observation of depolarized ZnO(0001) monolayers: formation of unreconstructed planar sheets *Phys. Rev. Lett.* **99** 026102
- [28] Li J, Gui G and Zhong J 2008 Tunable bandgap structures of two-dimensional boron nitride *J. Appl. Phys.* **104** 094311
- [29] Lee G H *et al* 2011 Electron tunneling through atomically flat and ultrathin hexagonal boron nitride *Appl. Phys. Lett.* **99** 243114
- [30] Balu R, Zhong X, Pandey R and Karna S P 2012 Effect of electric field on the band structure of graphene/boron nitride and boron nitride/boron nitride bilayers *Appl. Phys. Lett.* **100** 052104
- [31] Hohenberg P and Kohn W 1964 Inhomogeneous electron gas *Phys. Rev.* **136** B864–71
- [32] Soler M *et al* 2002 The SIESTA method for *ab initio* order-N materials *J. Phys.: Condens. Matter* **14** 2745–79
- [33] Perdew J P, Burke K and Ernzerhof M 1996 Generalized gradient approximation made simple *Phys. Rev. Lett.* **77** 3865–8
- [34] Kim K, Lambrecht W and Segall B 1996 Elastic constants and related properties of tetrahedrally bonded BN, AlN, GaN, and InN *Phys. Rev. B* **53** 16310–26
- [35] Christensen N E and Gorczyca I 1994 Optical and structural properties of III–V nitrides under Pressure *Phys. Rev. B* **50** 4397
- [36] Fritsch D, Schmidt H and Grundmann M 2003 Band-structure pseudopotential calculation of zinc-blende and wurtzite AlN, GaN, and InN *Phys. Rev. B* **67** 235205
- [37] Vurgaftman I and Meyer J R 2003 Band parameters for nitrogen-containing semiconductors *J. Appl. Phys.* **94** 3675
- [38] Silveira E *et al* 2004 Near-bandedge cathodoluminescence of an AlN homoepitaxial film *Appl. Phys. Lett.* **84** 3501
- [39] Sachs B, Wehling T O, Katsnelson M I and Lichtenstein A I 2011 Adhesion and electronic structure of graphene on hexagonal boron nitride substrates *Phys. Rev. B* **84** 195414
- [40] Grimsditch M, Zouboulis E S and Polian A 1994 Elastic constants of boron nitride *J. Appl. Phys.* **76** 832–4
- [41] Ueno M, Onodera A and Shimomura O 1992 X-ray observation of the structural phase transition of aluminum nitride under high pressure *Phys. Rev. B* **45** 10123
- [42] Perlin P, Gorczyca I, Porowski S and Suski T 1993 III–V semiconducting nitrides: physical properties under pressure *Japan. J. Appl. Phys.* **32** 334–9
- [43] Britnell L *et al* 2012 Atomically thin boron nitride: a tunnelling barrier for graphene devices *Nano Lett.* **12** 1707–10